JOURNAL OF SOLID STATE CHEMISTRY **140,** 377–386 (1998)
ARTICLE NO. SC987904

Synthesis, Phase Diagram, and Conductivity Study in a $La_{0.5+x+y}Li_{0.5-3x}Ti_{1-3y}Mn_{3y}O_3$ System

I. Moreno, M. Morales, and M. L. Martínez Sarrión[1]

Deptartment of Inorganic Chemistry, Universitat de Barcelona, Diagonal 647, 08028, Spain

Received November 11, 1997; revised May 20, 1998; accepted May 22, 1998

The stoichiometry, polymorphysm, and electrical behaviour of solid solutions of $La_{0.5+y+x}Li_{0.5-3x}Ti_{1-3y}Mn_{3y}O_3$ with perovskite-type structure have been studied. Data are given in the form of a solid solution triangle, phase diagrams, XRD patterns for the three polymorphs, A, β, and C, composition-dependence of their lattice parameters, and ionic and electronic conductivity plots. Microstruture and composition were studied by SEM/EDS and electron probe microanalysis. These compounds are mixed conductors. Ionic conductivity decreases when the amount of lithium diminishes and electronic conductivity increases with manganese content. © 1998 Academic Press

Key Words: **mixed conductors; crystal chemistry; phase diagram.**

INTRODUCTION

Research into solid ionic conductors and lithium cathodes is important for the development of solid state lithium batteries. For some time, research focused on doping compounds such as Li_4XO_4 and Li_3YO_4 (X = Si, Ge, Ti; Y = P, As, V) (1–4). Then a few years ago, fast ion conductors with the general formula $Li_{0.5-3x}RE_{0.5+x}TiO_3$, where RE = La, Pr, Nd, and Sm were reported (5–7). The maximum bulk conductivity was found in the lanthanum system, with a value of 1.1×10^{-3} Scm^{-1} for $x = 0.07$, although the total conductivity was less than 10^{-6} Scm^{-1}. More recently, the phase diagram, crystal chemistry and ion conductivity of the system $Li_{0.5-3x}RE_{0.5+x}TiO_3$ (RE = La, Pr, Nd) (8–11), which shows a similar total conductivity, have been reported.

The aim of the present work is to investigate the stoichiometry range, thermal stability, crystal chemistry, and electrical behavior of the materials of the general formula $Li_{0.5-3x}La_{0.5+x+y}Ti_{1-3y}Mn_{3y}O_3$. Since $Li_{0.5-3x}La_{0.5+x}TiO_3$ compounds are the best Li^+-ion conductors and manganese oxides with perovskite structure show high electronic conductivity, the partial substitution of titanium by manganese in these compounds could lead to mixed conductors with high ionic and electronic conductivity.

EXPERIMENTAL

La_2O_3 (99.9% Fluka), TiO_2 (Aldrich 99 + %), MnO_2 (>99% Fluka), and Li_2CO_3 (Aldrich > 99%) were used as starting materials. La_2O_3 and TiO_2 were dried overnight at 900°C prior to weighing. These chemicals were weighed, mixed in an agate mortar with acetone, dried, and heated at 650°C for 2 h to drive off CO_2. After grinding, samples were pressed into pellets and covered with powder of the same composition to avoid losing lithium during the thermal treatment. The pellets were fired at 1100°C for 8 h giving green products which were reground, repelleted, and fired at 1200° and 1250°C for 12 . A further treatment was carried out on samples richer in manganese ($y > 0.7$) at 1400°C for 2 h to spread the single phase region.

Phase diagram studies versus temperature were carried out for certain compounds. Small pelleted samples were wrapped in platinum foil envelopes, placed in a furnace, and annealed isothermally for 15 min in order to reach equilibrium. Finally they were dropped in liquid nitrogen to quench phase.

The solid solution range, crystalline phase identification, and lattice parameters were obtained by powder X-ray diffraction with a Siemens D-500 diffractometer in reflection mode and an INEL ENRAF NONIUS FR590 diffractometer in transmission mode with a psd-120° detector and a graphite monochromator, using $K\alpha$Cu. Lattice parameters were obtained using a silicon internal standard.

Some samples were studied by EPMA to verify homogeneity with a Cameca SX50 EPMA instrument. Elemental maps were obtained with a AN10000 EDS coupled to a JEOL JSM-840 microscope. Stoichiometry was obtained by ICP with a JOVIN IVON. DC measurements were carried out using an HP 3435A multimeter, and AC measurements with an HP 4192A Impedance Analyser over the range $5\ Hz < f < 1.3\times10^7$ Hz. Data corrections were

[1] Corresponding author.

0022-4596/98 $25.00

carried out in order to avoid stray inductance, although data above 5×10^6 Hz were discarded.

RESULTS AND DISCUSSION

Solid Solutions Diagram

The triangle $LaMnO_3$–$La_{0.5}Li_{0.5}TiO_3$–$La_{0.66}TiO_3$ in the system Li_2O–La_2O_3–TiO_2–Mn_2O_3 was chosen for a detailed study since the join $La_{0.5}Li_{0.5}TiO_3$–$La_{0.66}TiO_3$ has been reported elsewhere (8) and $LaMnO_3$ has a similar structure to compounds on this join.

This triangle was studied by synthesizing compositions of the general formula $Li_{0.5-3x}La_{0.5+x+y}Ti_{1-3y}Mn_{3y}O_3$ in the heating conditions described above. The results were used to construct the composition diagram shown in Fig. 1.

Three distinct areas were found on this triangle. A large region of perovskite-like solid solutions and two regions of mixed phases (Fig. 2). The region that was within vertex $Li_{0.5}La_{0.5}TiO_3$ was a mixture of perovskite-like compound, Li_2TiO_3, and an unknown phase, while the region closest to the vertex $La_{0.66}TiO_3$ was a mixture of a perovskite-like phase, $La_2Ti_2O_7$ and TiO_2.

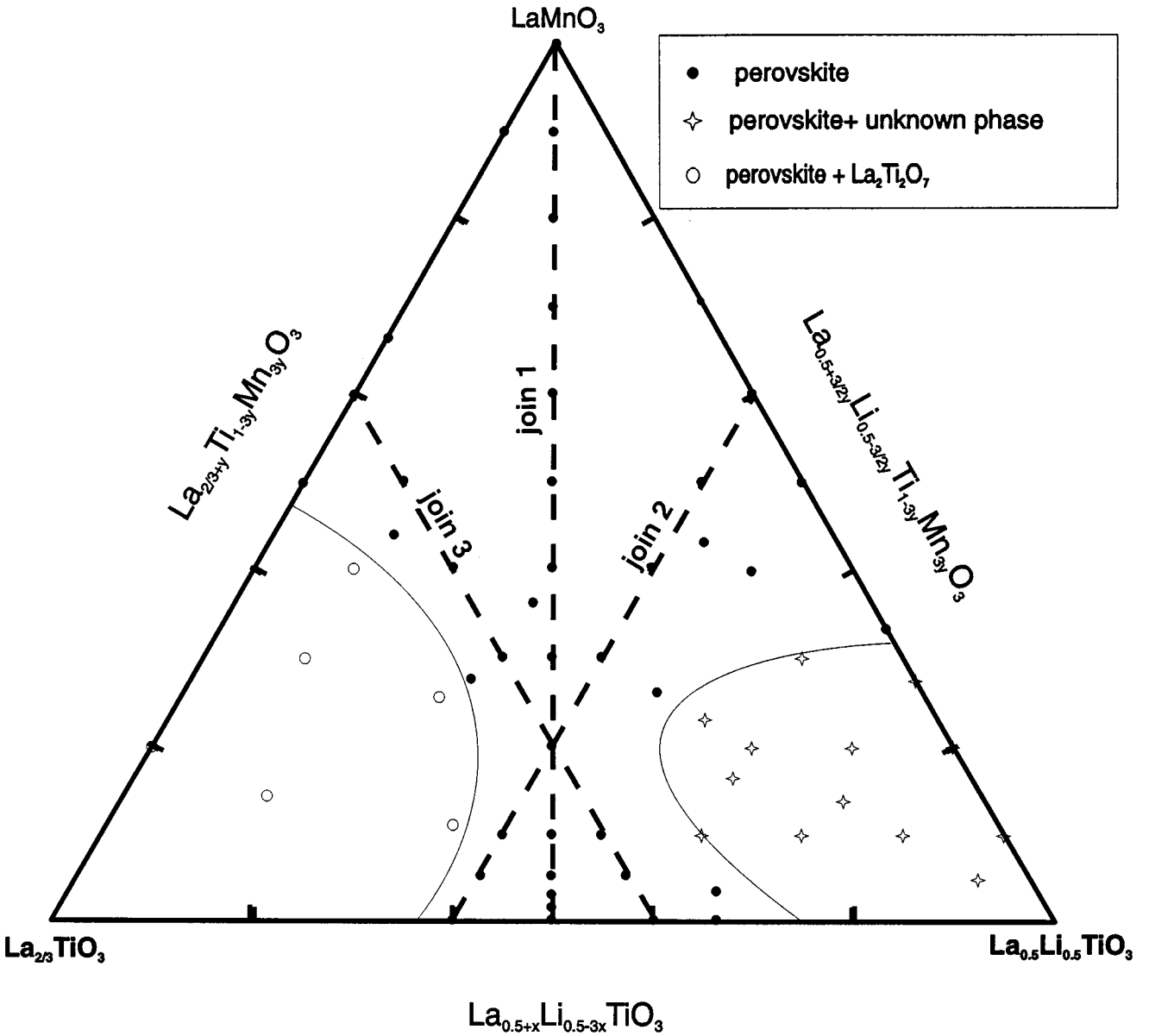

FIG. 1. Composition triangle and joins studied of the system $La_{0.5+x+y}Li_{0.5-3x}Ti_{1-3y}Mn_{3y}O_3$.

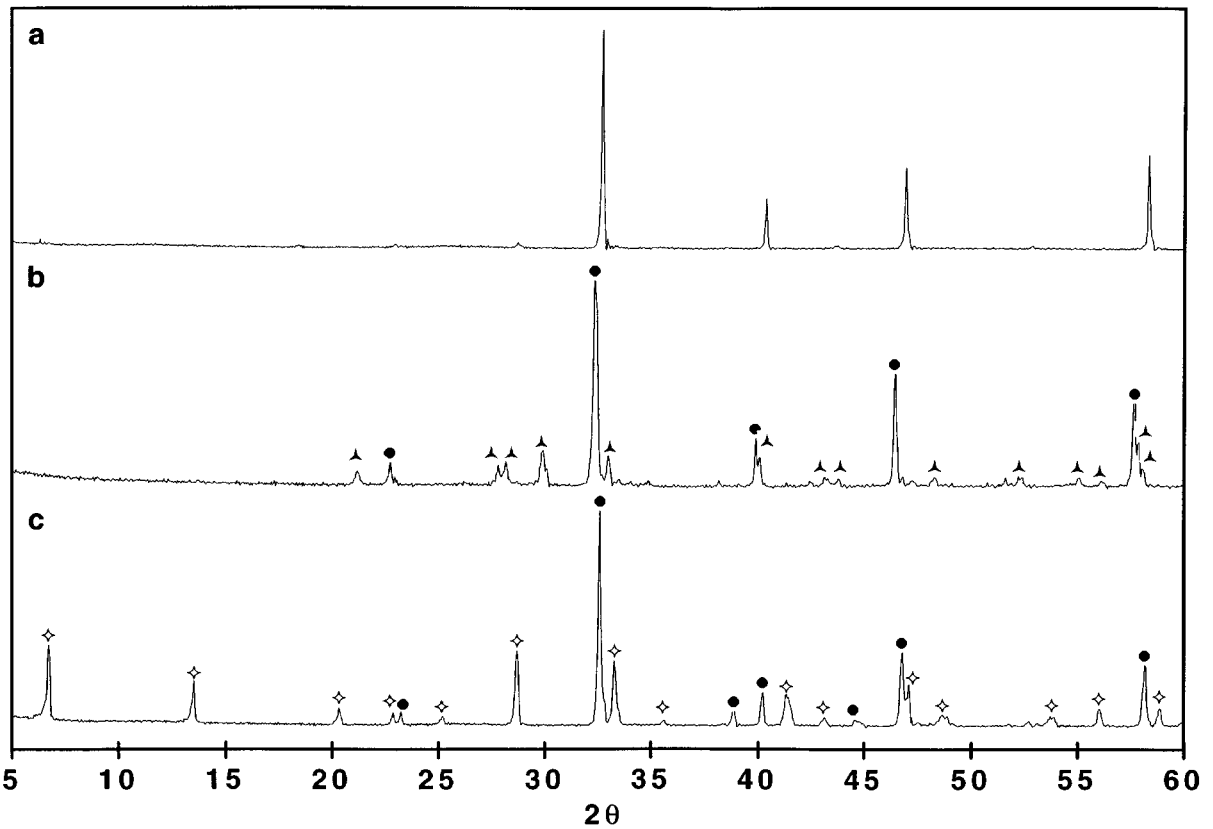

FIG. 2. XRD patterns of the three regions on the composition triangle: (a) single phase solid solution region; (b) perovskite-like phase (●) + $La_2Ti_2O_7$ (▲) region; and (c) perovskite-like phase (●) + unknown phase (◇) region.

Electron Probe Microanalysis (EPMA) and Scanning Electon Microscopy (SEM)

A number of samples from the three regions observed in the composition triangle were studied by EPMA and SEM/EDS to obtain element analyses and elemental maps. Element analyses were carried out with a fixed beam of 15 kV and 20 nA over 15 different points of the sample surface, with $SrTiO_3$, LaB_6, and Rhodochrosite as standards for Ti and O, La, and Mn, respectively. Lithium content could not be obtained directly and so it had to be calculated by assuming three oxygen atoms per unit formula and valencies of 3+ for La and Mn and 4+ for Ti. The element maps of Ti, La, and Mn were produced with an electron beam of 15 kV and 20 nA, using a LINK AN10000 EDS coupled to a JEOL JSM-840 microscope.

Element maps were obtained for three samples from each of the three regions observed in the composition triangle. Figure 3 shows a secondary electron image, SEI, and La, Ti, and Mn maps for $La_{0.833}Li_{0.10}Ti_{0.40}Mn_{0.60}O_3$ (*single phase region*). Only one phase, with a homogeneous element distribution was found; dark areas represent porosity.

Element maps for $La_{0.69}Li_{0.07}Ti_{0.86}Mn_{0.14}O_3$ (Fig. 4a and 4b) showed the presence of at least two phases. Light area on SEI indicated a rich region in La that can be attributed to $La_2Ti_2O_7$ compound; while dark spots correspond to a perovskite compound.

Secondary electron image and back-scattered electron image on $La_{0.593}Li_{0.36}Ti_{0.86}Mn_{0.14}O_3$ (Figs. 4c and 4d) showed two regions of composition. The large dark region corresponds to a perovskite compound, while light areas correspond to an unknown phase which was richer in heavy elements. Element maps of these areas did not show any significant differences in element distribution.

The results of element analyses on mixed regions (Table 1) for different spots matched those for the proposed compounds in Fig. 2.

Phase Diagrams and Crystal Chemistry

Phase diagrams and cell volume were obtained for three joins on the composition triangle (Fig. 1). Along join 1 [$La_{0.538}Li_{0.25}TiO_3$-$LaMnO_3$], lithium and lanthanum composition and the number of vacancies changed, while along join 2 [$La_{0.60}Li_{0.20}TiO_3$–$La_{0.80}Li_{0.20}Ti_{0.40}Mn_{0.60}O_3$],

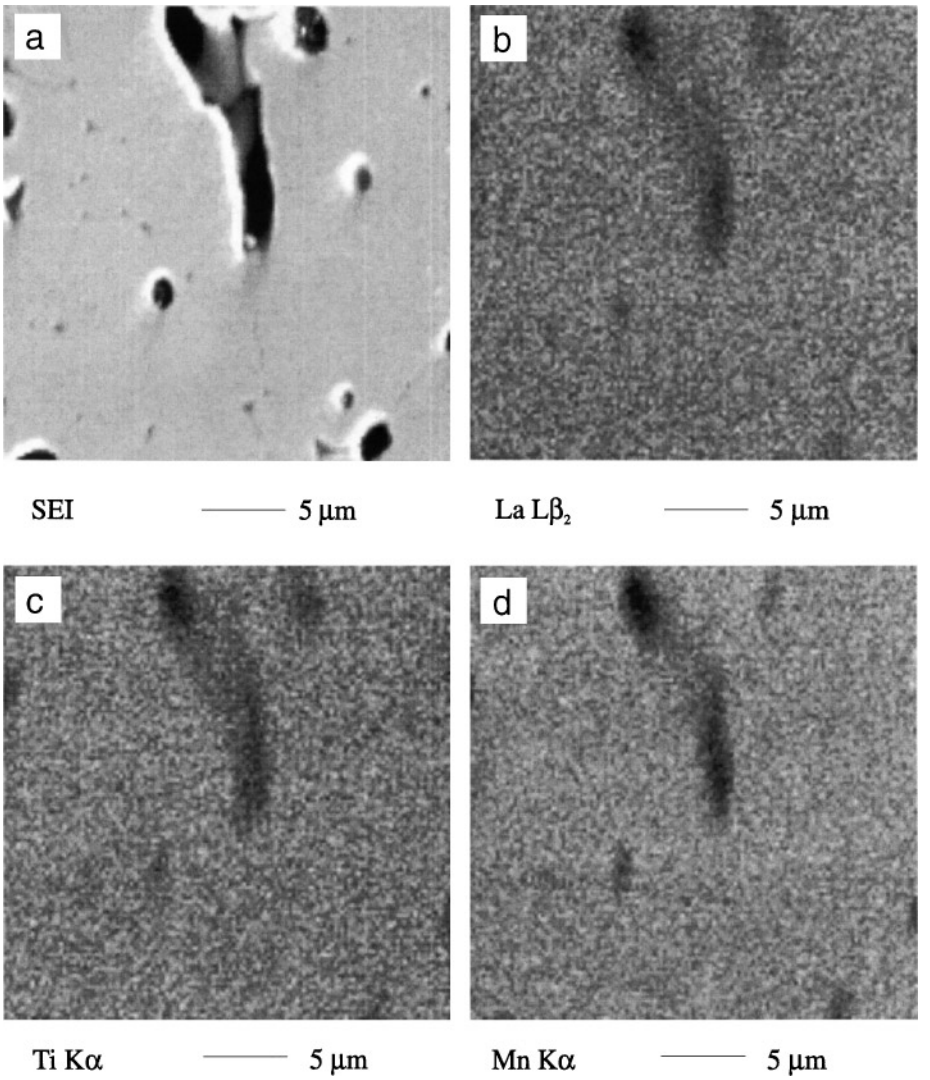

FIG. 3. SEI and elemental maps for $La_{0.833}Li_{0.10}Ti_{0.40}Mn_{0.60}O_3$ (single phase region): (a) SEI, (b) elemental map of La, (c) map of Ti, and (d) map of Mn.

TABLE 1
Element Analyses by EPMA on Multiphase Regions

Starting materials					Experimental values			
La	Ti	Mn	Li	Spots	La	Ti	Mn	O
0.60	0.80	0.20	0.40	Dark[a]	0.58(1)	0.83(1)	0.17(1)	2.9(1)
				Light	0.67(2)	0.81(1)	0.18(1)	2.91(7)
0.593	0.86	0.14	0.36	Dark[a]	0.57(2)	0.86(2)	0.14(2)	2.8(2)
				Light	0.63(1)	0.87(2)	0.13(2)	2.9(2)
0.71	0.74	0.26	0.13	Dark[b]	0.70(1)	0.738(9)	0.26(1)	2.85(9)
				Light	0.96(1)	0.95(2)	0.051(9)	3.3(2)
0.69	0.86	0.14	0.07	Dark[b]	0.65(1)	0.849(9)	0.15(1)	2.9(1)
				Light	0.95(1)	0.97(5)	0.02(5)	3.3(1)

[a] EPMA on samples placed in the region of mixtures of perovkite-related phases and unknown phase. *Dark* and *light spots* are in relation to secondary electron images.

[b] EPMA on samples placed in the region of mixtures of perovkite-like phases and $La_2Ti_2O_7$. *Dark* and *light spots* are in relation to backscattered electron images.

TABLE 2
X-Ray Powder Diffraction Data for $La_{0.70}Li_{0.20}Ti_{0.70}Mn_{0.30}O_3$ Quenched from 900°C (Phase A)

h k l	d_{obs}	d_{calc}	I/I_o
1 0 0	3.8812	3.880	9
1 1 0	2.744	2.7438	100
1 1 1	2.2404	2.2403	20
2 0 0	1.9401	1.9402	34
2 1 0	1.7355	1.7353	4
2 1 1	1.5839	1.5841	28
2 2 0	1.3717	1.3719	13
3 0 0	1.2934	1.2934	2
3 1 0	1.2272	1.2271	9

Note. Cubic system: $a_o = 3.8803(4)$ Å, $V = 58.420(1)$ Å^3, $Z = 1$.

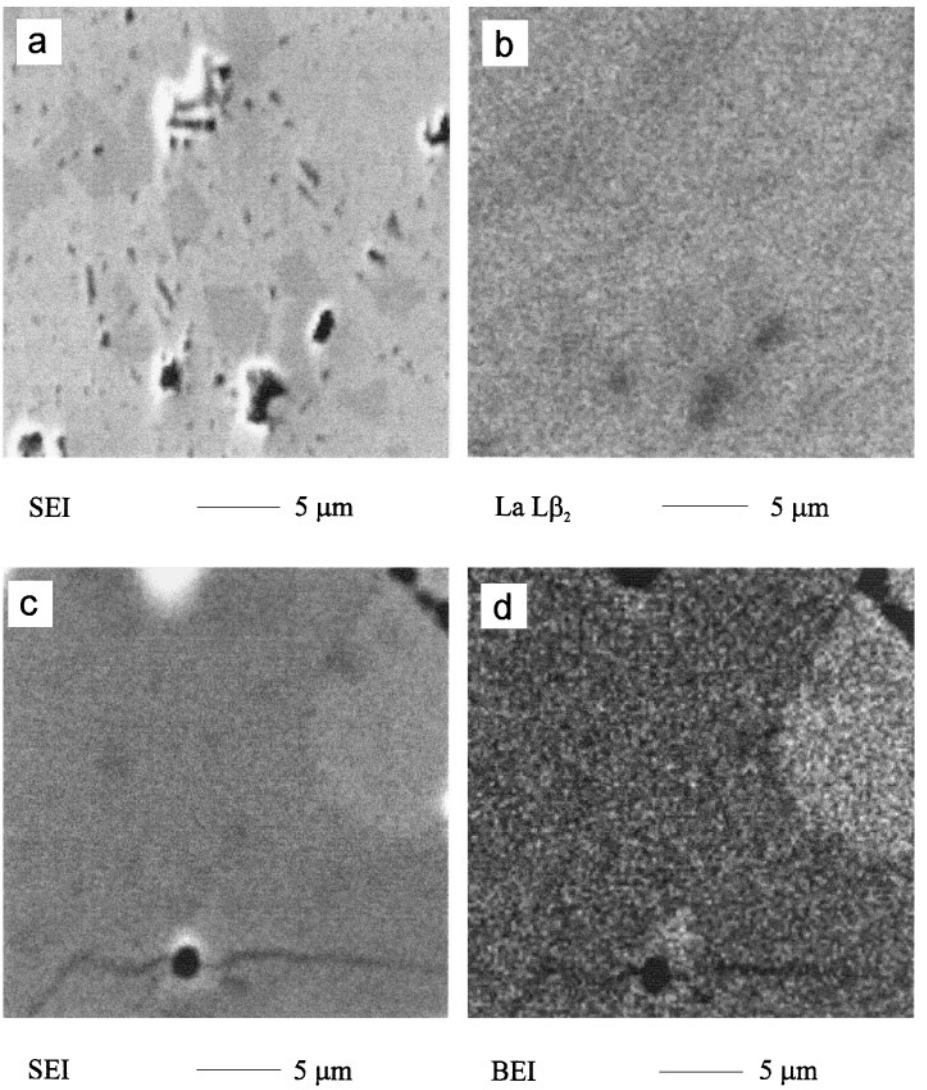

FIG. 4. Elemental maps of multiphase regions: (a) SEI and (b) map of La of $La_{0.69}Li_{0.07}Ti_{0.86}Mn_{0.14}O_3$, and (c) SEI and (d) BEI of $La_{0.593}Li_{0.36}Ti_{0.86}Mn_{0.14}O_3$.

the amount of lithium was constant and along the join 3 [$La_{0.567}Li_{0.30}TiO_3$–$La_{0.86}Ti_{0.40}Mn_{0.60}O_3$], the number of vacancies was constant.

Three polymorphs, labelled A, C, and β (Fig. 5), by analogy with similar polymorphs in the $RE_{0.5+x}Li_{0.5-3x}TiO_3$ (RE = Pr and Nd) (8, 9) systems, were identified. These three polymorphs have a perovskite-related structure given the similarity in their XRD patterns (Fig. 6).

The polymorph A is a simple cubic perovskite (Table 2) and the polymorph C (Table 3) is an orthorhombic distortion of A, with a unit cell which is approximately four times larger. The cells of A and C are related by: $a_o = \sqrt{2}a_c + \delta$, $b_o = 2a_c$, and $c_o = \sqrt{2}a_c - \delta$, where a_c is the cell parameter of the cubic A phase and δ is the degree of orthorhombicity. The polymorph β is a tetragonal perovskite with unit cell: $a_o = a_c - \delta$ and $c_o = 2a_c + \Delta$ (Table 4).

Polymorphs A and C only form at high temperatures; phase C for a small number of vacancies in the structure and phase A for a large number. Although, these phases are stable at high temperatures, they can, nevertheless, be preserved at room temperature by quenching. The polymoph C, which is absent in the system $La_{0.5+x}Li_{0.5-3x}TiO_3$, appears when titanium is partially substituted by manganese. The polymoph β extends along the whole range of compositions on the three joins at low temperatures.

Cell volume was measured against the amount of lanthanum along these three joins (Fig. 7) and was found to

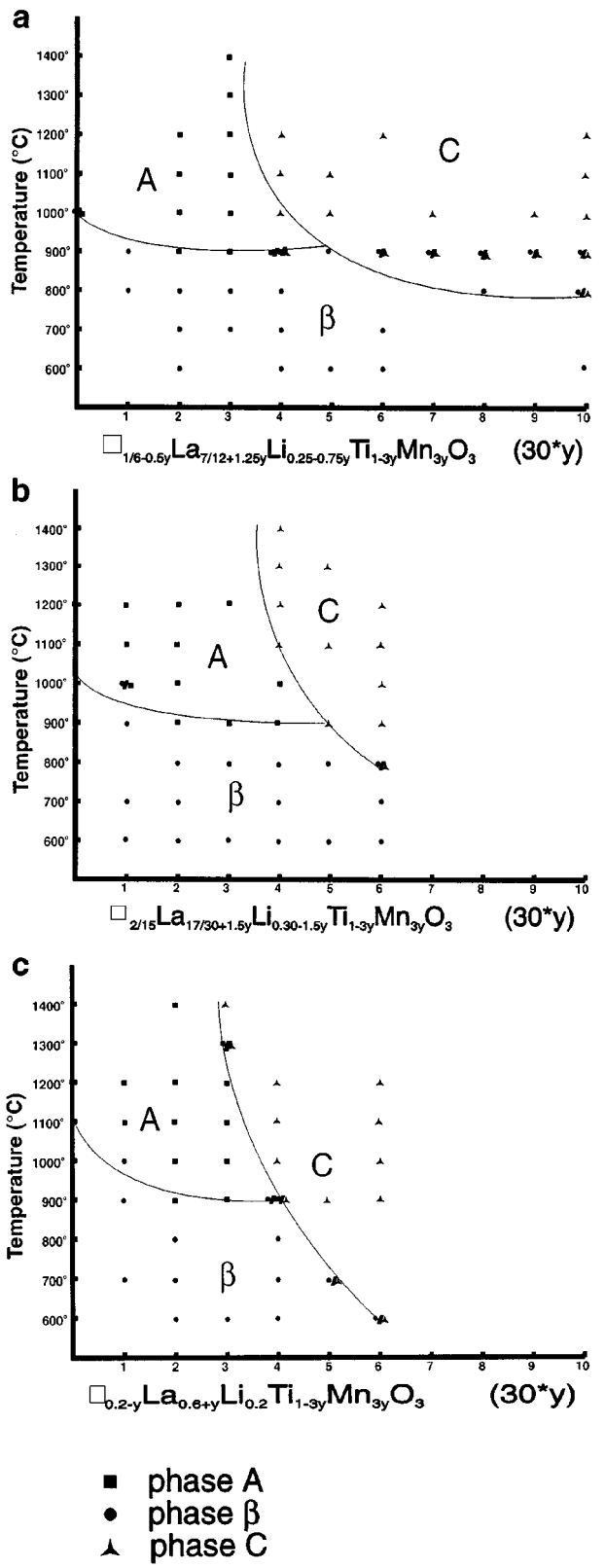

FIG. 5. Phase diagrams along each join: (a) $La_{0.538}Li_{0.25}TiO_3$–$LaMnO_3$ (b) $La_{0.60}Li_{0.20}TiO_3$–$La_{0.80}Li_{0.20}Ti_{0.40}Mn_{0.60}O_3$, and (c) $La_{0.567}Li_{0.30}TiO_3$–$La_{0.86}Ti_{0.40}Mn_{0.60}O_3$.

TABLE 3
X-Ray Powder Diffraction Data for $La_{0.767}Li_{0.20}Ti_{0.50}Mn_{0.50}O_3$ Quenched from 1100°C (Phase C)

h k l	d_{obs}	d_{calc}	I/I_o
0 0 2	3.8961	3.8891	14
2 0 0	2.7584	2.7627	100
1 1 2	2.7494	2.7505	97
2 1 1	2.3507	2.3506	2
1 0 3	2.3448	2.3471	1
2 0 2	2.2524	2.2520	28
0 2 2	2.2396	2.2398	10
0 0 4	1.9480	1.9446	58
3 0 1	1.7914	1.7920	1
3 1 0	1.7455	1.7456	3
2 2 2	1.7400	1.7398	3
1 3 0	1.7357	1.7342	2
3 1 2	1.5922	1.5925	29
2 0 4	1.5883	1.5901	14
0 2 4	1.5849	1.5858	8
4 0 0	1.3808	1.3811	9
2 2 4	1.3749	1.3753	10
0 4 0	1.3710	1.3699	4
4 0 2	1.3016	1.3015	< 1
3 1 4	1.2989	1.2990	1
0 0 6	1.2957	1.2964	2
1 3 4	1.2946	1.2943	< 1
0 4 2	1.2898	1.2921	< 1
4 2 0	1.2341	1.2333	< 1
1 1 6	1.2309	1.2299	9
2 4 0	1.2279	1.2273	4

Note. Orthorhombic system: $a_o = 5.524(5)$ Å, $b_o = 5.479(5)$ Å, $c_o = 7.778(7)$ Å, $V = 235.47(4)$ Å^3, $Z = 4$.

increase whenever the lanthanum content increased, while for the same amount of lanthanum, it decreased as the lithium content increased. Since both lithium and lanthanum should be in 12-coordinated sites, steric effects are predominant in lanthanum substitution, making the cells larger, while electrostatic interaction between lithium and octahedrons is more important in lithium substitution, with the reverse effect on the cells.

Electrical Measurements (AC/DC)

An HP 4192A analyzer were used for AC measurement, and an HP 3435A multimeter for DC measurements. These measurements were carried out from 0°C to 100°C for compounds on join 1. Along this join, three types of behavior were shown. For $y = 0.0$, only ionic conductivity and two semicircles and a spike were observed. The centre of these semicircles was depressed below the baseline, indicating a non-Debye response, which is usual in ionic conductors (12, 13). For $0 < y \leq 0.067$, compounds were

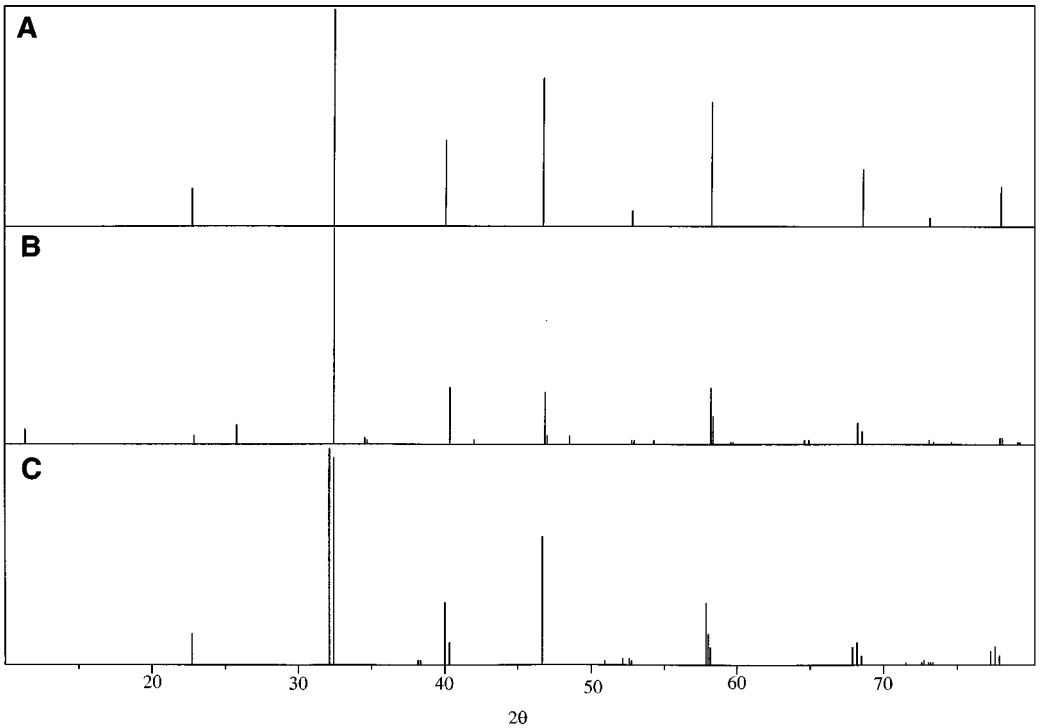

FIG. 6. XRD patterns of: (a) $La_{0.70}Li_{0.20}Ti_{0.70}Mn_{0.30}O_3$ quenched from 900°C in N_2 (polymorph A); (b) $La_{0.667}Li_{0.20}Ti_{0.80}Mn_{0.20}O_3$, quenched from 700°C (polymorph β); and (c) $La_{0.767}Li_{0.20}Ti_{0.50}Mn_{0.50}O_3$ quenched from 1100°C (polymorph C).

mixed conductors with greater ionic than electronic conductivity and three semicircles were observed. The third semicircle became smaller as the electronic conductivity was increased. Finally, for $y > 0.3$, electronic conductivity was greater than ionic conductivity, and only two semicircles were observed.

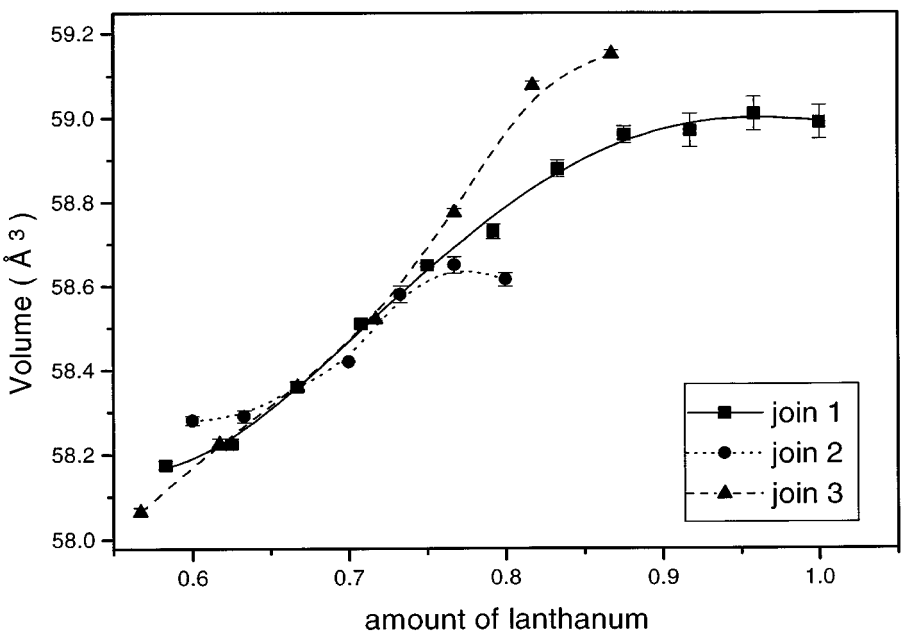

FIG. 7. Cell volume vs composition in lanthanum along the three joins on samples quenched from 900°C.

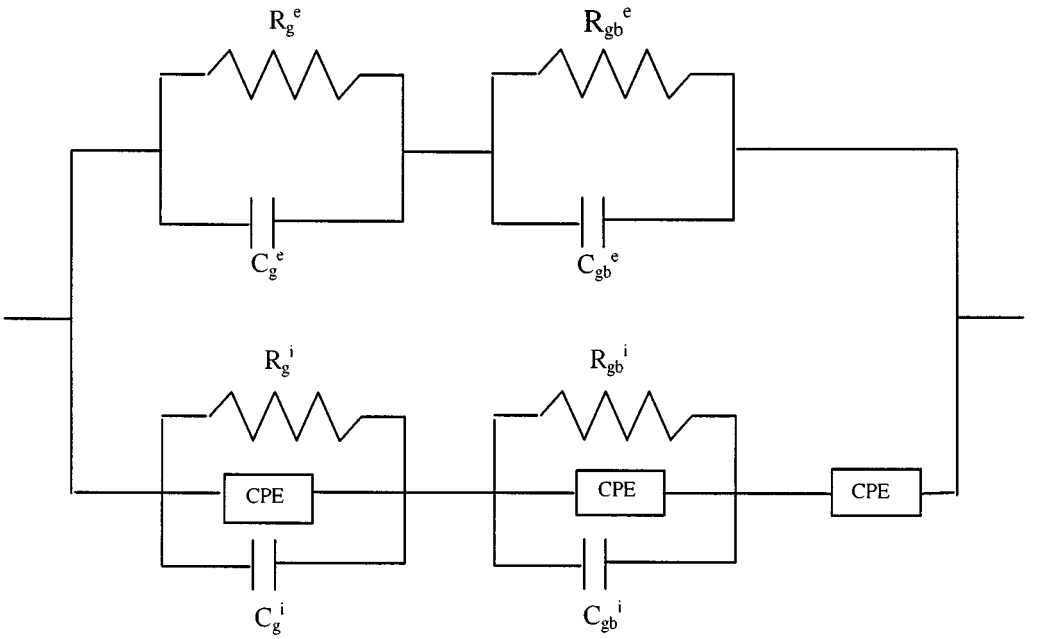

FIG. 8. Equivalent circuit for fitting AC data.

TABLE 4
X-Ray Powder Diffraction Data for $La_{0.667}Li_{0.20}Ti_{0.80}Mn_{0.20}O_3$ Quenched from 700°C (Phase β)

h k l	d_{obs}	d_{calc}	I/I_o
0 0 1	7.7638	7.7632	7
0 0 2	3.8742	3.8816	5
0 1 1	3.4639	3.4647	9
1 0 2	2.7411	2.7411	100
0 0 3	2.5840	2.5840	3
1 1 1	2.6002	2.5818	2
1 1 2	2.2353	2.2372	26
0 1 3	2.1536	2.1514	2
0 0 4	1.9377	1.9408	24
2 0 0	1.9164	1.9358	4
1 1 3	1.8811	1.8806	4
1 0 4	1.7339	1.7350	2
2 1 0	1.7296	1.7314	1
2 1 1	1.6906	1.6899	2
1 1 4	1.5831	1.5833	26
1 2 2	1.5792	1.5813	13
0 0 5	1.5517	1.5526	1
2 0 3	1.5479	1.5501	1
0 1 5	1.4431	1.4411	1
2 1 3	1.4400	1.4390	1
0 2 4	1.3716	1.3706	10
2 2 0	1.3682	1.3688	5
0 0 6	1.2930	1.2939	2
2 1 4	1.2897	1.2920	1
2 2 2	1.2904	1.2909	< 1
3 0 1	1.2736	1.2731	< 1
1 0 6	1.2290	1.2272	3
3 0 2	1.2261	1.2246	4
3 1 0	1.2248	1.2243	3
2 0 5	1.2115	1.2112	1
3 1 1	1.2084	1.2094	1

Note. Tetragonal system: $a_o = 3.871(4)$ Å, $c_o = 7.763(9)$ Å, $V = 116.36(8)$ Å^3, $Z = 2$.

An equivalent circuit (Fig. 8) with two parallel branches, one of them related to ionic conductivity and the other one to electronic conductivity, has been used to fit experimental measurements. The electronic part is comprised of two RC elements associated to grain and grain boundary responses, while the ionic part was made of two RC elements with two CPE (constant phase elements) (14) for grain and grain boundary response and an additional CPE element to model a blocking electrode for lithium ions. All fittings used the Zview software package (15).

Overall the electronic conductivity, DC measurements, showed that samples doped with small amounts of manganese became mixed conductors. Although the electronic

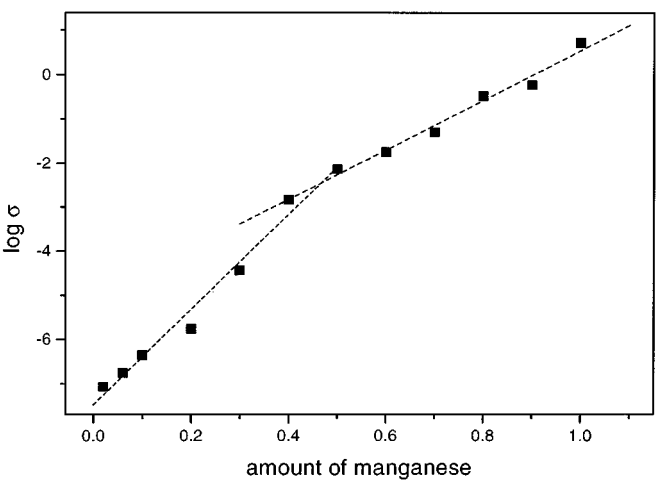

FIG. 9. Plot of log σ (overall electronic conductivity) vs composition in manganese along join 1 [$La_{0.538}Li_{0.25}TiO_3$–$LaMnO_3$].

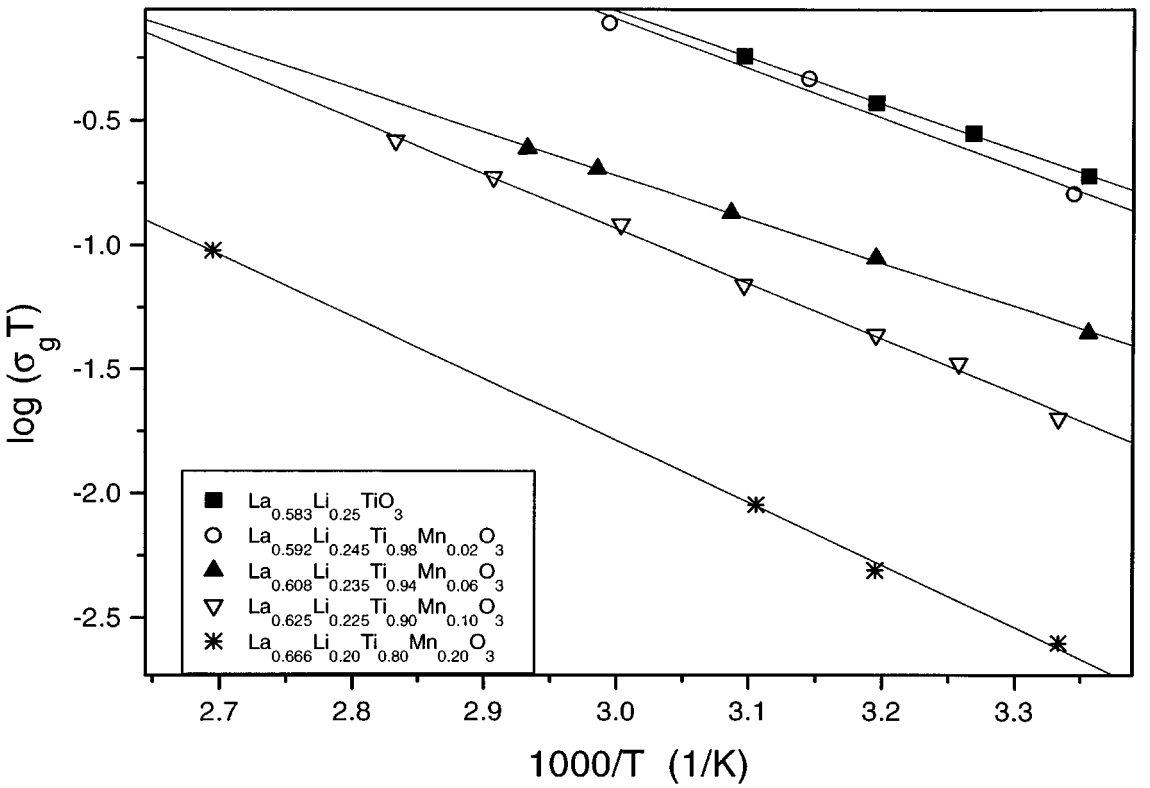

FIG. 10. Arrhenius ionic conductivity plots.

conductivity was highly dependent on manganese content (Fig. 9), it seems that titanium must play a role, since samples with $y = 0.007$ were electronic conductors and the amount of manganese was very small. The plot *log σ vs manganese amount* (Fig. 9) showed an inflexion point at $y = 0.133$, suggesting that there were probably two

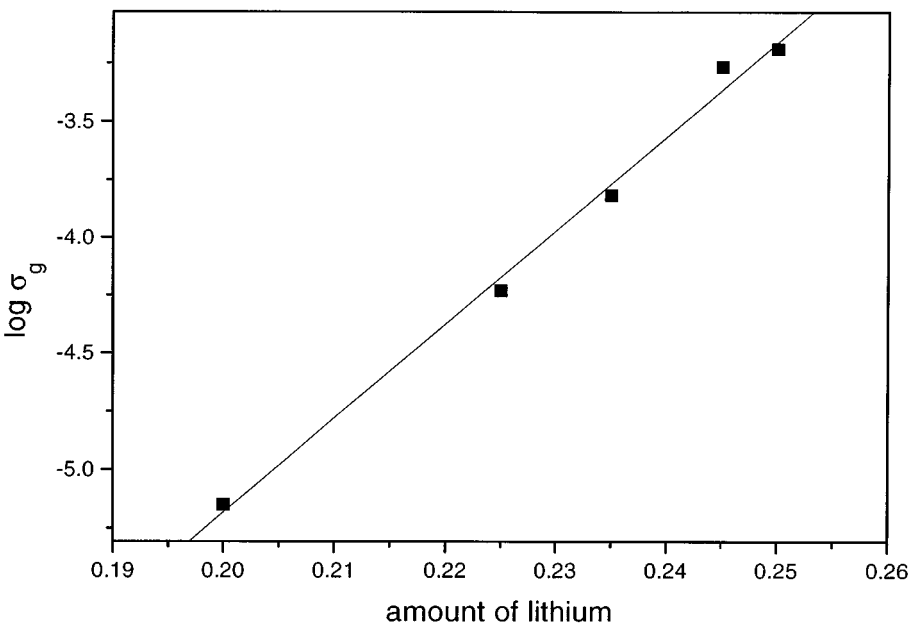

FIG. 11. Plot of log σ (bulk ionic conductivity) vs composition in lithium along join 1 [$La_{0.538}Li_{0.25}TiO_3$–$LaMnO_3$].

mechanisms associated with electronic conductivity. For $y > 0.133$, manganese is probably responsible for the electronic conductivity, while for $y < 0.133$, manganese and titanium intervened in the electronic conductivity.

Bulk ionic conductivity data from the impedance complex plane plots are shown in Arrhenius format. The plots are linear and the conductivity decreased as the amount of lithium diminished (Fig. 10). The variation in ionic conductivity with the lithium composition is quite large (Fig. 11), although ionic and electronic conductivity remained similar for $y = 0.01$.

ACKNOWLEDGMENT

This work was partially sponsored by financial support from CICYT MAT95-0218.

REFERENCES

1. H. Y. P. Hong, *Mater. Res. Bull.* **13,** 117 (1978).
2. M. A. K. L. Dissanayake and A. R. West, *J. Mater. Chem.* **1**(6), 1023 (1991).
3. C. K. Lee and A. R. West, *J. Mater Chem.* **1**(1), 149 (1991).
4. A. Robertson and A. R. West, *Solid State Ionics* **58,** 351 (1992).
5. M. Itoh, Y. Inaguma, W. Jung, L. Chen, and T. Nakamura, *Solid State Ionics* **70/71,** 203 (1994).
6. H. Kawai and J. Kuwano, *J. Electrochem. Soc.* **141**(7), L78 (1994).
7. Y. Inaguma, L. Chen, M. Itoh, and T. Nakamura, *Solid State Ionics* **70/71,** 196 (1994).
8. A. D. Robertson, S. García Martín, A. Coats, and A. R. West, *J. Mater. Chem.* **5**(9), 1405 (1995).
9. M. Morales and A. R. West, *Solid State Ionics* **84,** 33 (1996).
10. J. M. S. Skakle, G. C. Mather, M. Morales, R. I. Smith, and A. R. West, *J. Mater. Chem.* **5**(11), 1807 (1995).
11. R. I. Smith, J. M. S. Skakle, G. C. Mather, M. Morales, and A. R. West, *Mater. Sci. Forum* **228–231,** 701 (1996).
12. A. K. Jonscher and J. M. Reau, *J. Mater. Sci.* **13,** 563 (1978).
13. P. G. Bruce, A. R. West, and D. P. Almond, *Solid State Ionics* **7,** 57 (1982).
14. A. K. Jonscher, *in* "Dielectric Relaxation in Solids," Chap. 5. Chelsea Dielectrric, London, 1983.
15. Zview for Windows (Version 1.4), Scribner, Charlotesville, VA.